JOURNAL OF MATERIALS SCIENCE **37** (2002) 2129–2141

Fly ash reactivity: Extension and application of a shrinking core model and thermodynamic approach

H. J. H. BROUWERS, R. J. VAN EIJK
Department of Civil Engineering, University of Twente, P.O. Box 217, 7500 AE Enschede, The Netherlands
E-mail: h.j.h.brouwers@ctw.utwente.nl

In the present paper a theoretical study is presented on the dissolution (reaction) of pulverised powder coal fly ash. A shrinking core model is derived for hollow spheres that contain two regions (outer hull and inner region). The resulting analytical equations are applied to the dissolution experiments by Pietersen (Mat.Res.Soc.Symp.Proc., Vol. 178, Materials Research Society, 1990, p. 139; Ph.D. Thesis, Delft University of Technology, The Netherlands, 1993), yielding reaction rates at various temperatures and pH for two class F fly ashes. It is revealed that the available amount of reactive fly ash is proportional to the glass content of the fly ash, and that the reaction rate is proportional to this glass content as well. Moreover, it is concluded that the outer region is less reactive than the inner region, and that these reactivities are proportional to a power of the hydroxyl concentration. Subsequently, experimental data and model are used to assess the magnitude of inner and outer region. It seems that the outer hull of solid spheres and cenospheres are having the same thickness, about 2 μm. Based on the observed trends a reaction mechanism is proposed which accounts for the glass content and composition of the fly ash (and that is applicable to slags as well). Finally, using the reaction product, thermodynamic properties of the studied fly ashes are derived: the free energy, enthalpy and entropy of reaction.

1. Introduction

In the use and production of cement and concrete nowadays more and more secondary materials are employed such as pulverised coal fly ash, granulated blast furnace slag and silica fume. These products exhibit hydraulic and pozzolanic behaviour, i.e. they are able to react with water and water-dissolved calcium hydroxide (CH), respectively, to form pozzolanic C-S-H, a cement hydration product.

It is understood that the ability of secondary materials to react strongly depends on the alkali content and temperature of the water [1–6]. To investigate this, Pietersen [7, 8] performed pulverised coal fly ash dissolution experiments. During these experiments several pulverised fly ashes were dissolved in sodium hydroxide solutions of pH 13, 13.4 and 13.7, at various temperatures. As expected, dissolution rates (and related reaction rates as well) increased significantly with increasing pH and temperature.

As said, several authors have mentioned the relation between reaction rate at one hand and pH and temperature on the other hand. However, to the authors' knowledge, no analytical relation has been derived between reaction rate and pH and temperature. As this is of major importance to understand the hydration of cements blended with said secondary raw materials, in this paper such a relation is derived and applied.

First, a comprehensive model is presented of the dissolution of a sphere, using a shrinking core model approach as first proposed by Yagi and Kunii [9]. Here, the sphere is allowed to be hollow (to account for cenospheres) and to consist of two (concentric) regions (to account for different composition and reactivity). Subsequently, the resulting equations are applied to the experiments of Pietersen [7, 8]. Based on this application, a reaction equation for fly ash is put forward that contains the silica, aluminium oxide, alkali, alkaline earth, iron oxide and titanium oxide contents. From this application and proposed reaction mechanism the solubility of the fly ashes as a function of pH is obtained. The reaction mechanism and experiments of Pietersen [7, 8] are furthermore used to analyse the composition of the fly ash, in particular, the difference between the outer region (outer hull) and inner region. Finally, thermodynamic properties (such as the equilibrium constant and free energy of reaction) are determined of the considered fly ashes and compared with similar substances.

2. Experiments

Pietersen [7, 8] reported dissolution experiments with two different class F fly ashes ("EFA" and "LM") at pH = 13, 13.4 and 13.7. The dissolution experiments were executed at temperatures of 20°C, 30°C and 40°C. Sodium hydroxide (NaOH) was chosen as reaction

medium and each time 100 mg of fly ash was reacted with 100 ml of solution in sealed plastic bottles. Actually, the OH^- concentration (thus pOH) has been imposed, and the pH been determined via $pH + pOH = 14$ [10]. However, this relation is applicable only in case the temperature is 20°C and hence, here the pOH is used henceforth.

The two investigated fly ashes originate from two different power plants and have broad and mutually different particle size distributions. One power plant is a "wet-bottom" type plant that operates at 1800°C (EFA); the other fly ash originates from a low NO_x furnace plant (LM).

All experiments were executed with a sieved part of the fly ashes, the diameter lying between 38 μm and 50 μm. The fly ashes were also ultrasonically vibrated to prevent agglomeration of small particles to large ones. Moreover, for the experiments the particles were separated into a fraction of low density ("cenospheres") with a density smaller than 1400 kg/m^3 and in a fraction of high density ("solid spheres") with a density of 2300–2600 kg/m^3. SEM images of polished sections of these fractions revealed that the cenospheres were mainly hollow thin-walled spheres.

In Table I the most important properties of both fly ashes are summarised. In this table also the crystalline SiO_2 and Al_2O_3 that are part of the mullite are specified, using the molar masses of both substances ($M_A = 102$ g/mole, $M_S = 60$ g/mole) and considering that mullite contains (by mass) 306/426 Al_2O_3 and 120/426 silica.

The dissolution experiments were also executed with the hollow cenospheres and the solid spheres, which differ in density about a factor of two [7, 8]. The experiments revealed that for these two fly ashes Si, Al and K all dissolve congruently, implying bulk dissolution. Accordingly, the dissolution of the major component, Si, represents an adequate measure for the dissolution of the entire glass mass. This principle was used for the experiments, which are used here.

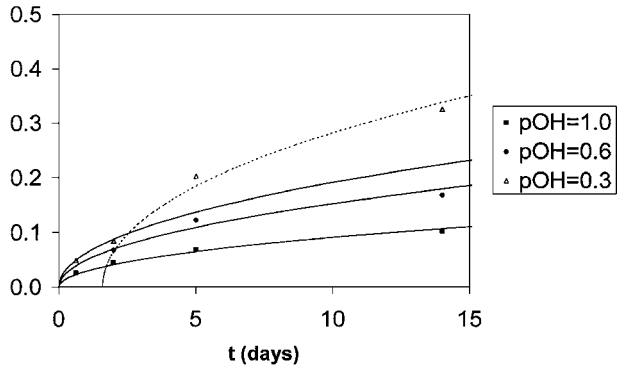

Figure 1 Fraction of mass dissolved z versus time [8] and fit (equations 31 and 32) for EFA solid spheres ($b = 1$) at pOH = 0.3, 0.6 and 1 ($T = 40$°C).

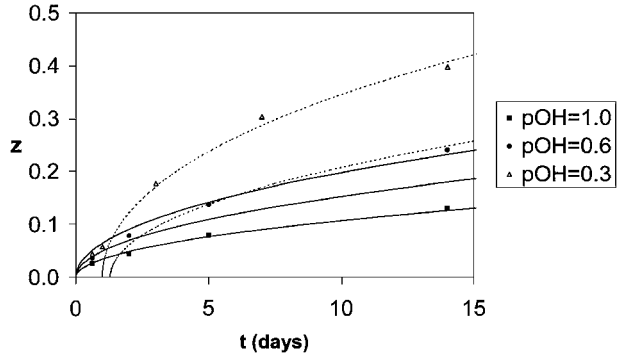

Figure 2 Fraction of mass dissolved z versus time [8] and fit (equations 31 and 32) for LM solid spheres ($b = 1$) at pOH = 0.3, 0.6 and 1 ($T = 40$°C).

In Figs 1 and 2 the fraction of the mass dissolved, z, at 40°C, is depicted against time for EFA and LM solid spheres, respectively, for three pOH levels. One can readily see that all experiments show a similar path

TABLE I Composition (in m/m%) of investigated fly ashes [8], specification of crystalline SiO_2 and Al_2O_3 in mullite (all percentages based on total fly ash mass)

	EFA		LM	
Overall composition	Solid	Ceno	Solid	Ceno
SiO_2 (S)	55.56%	51.55%	57.39%	52.21%
Al_2O_3 (A)	27.39%	31.96%	31.18%	39.54%
Fe_2O_3 (F)	4.65%	2.96%	3.50%	2.02%
TiO_2 (T)	1.20%	0.91%	1.90%	1.43%
MgO (M)	1.82%	1.41%	0.28%	0.24%
CaO (C)	2.83%	0.80%	2.75%	1.15%
Na_2O (N)	1.84%	1.94%	0.37%	0.38%
K_2O (K)	4.40%	5.68%	1.00%	1.02%
P_2O_5 (P)	n.d.	n.d.	0.54%	n.d.
H_2O (H)	0.3%	0.4%	1.1%	1.4%
LOI (carbon)	0.0%	2.4%	0.0%	0.6%
Of which:				
Mullite ($3Al_2O_3 \cdot 2SiO_2$)	2.1%	5.4%	20.5%	36.2%
Quartz (SiO_2)	3.0%	3.0%	12.8%	1.6%
	–	–	–	–
Total crystalline	5.1%	8.4%	33.3%	37.8%
Non-crystalline (ϕ)	94.9%	91.6%	66.7%	62.2%
Hence				
SiO_2 in mullite	0.6%	1.5%	5.8%	10.2%
Al_2O_3 in mullite	1.5%	3.9%	14.7%	26.0%

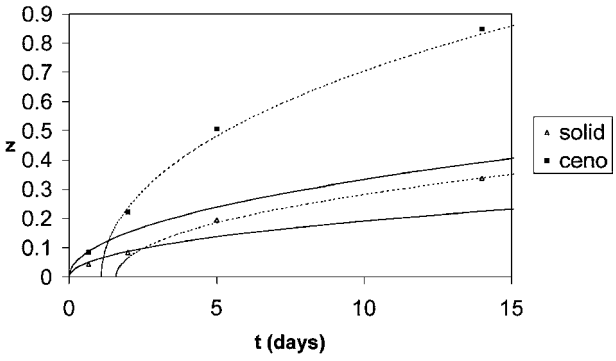

Figure 3 Fraction of mass dissolved z versus time [8] and fit (equations 31 and 32) for EFA cenospheres ($b = 0.5$) and solid spheres (pOH = 0.3, $T = 40°C$).

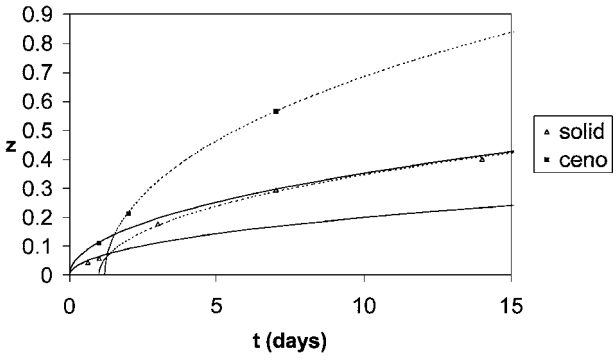

Figure 4 Fraction of mass dissolved z versus time [8] and fit (equations 31 and 32) for LM cenospheres ($b = 0.5$) and solid spheres (pOH = 0.3, $T = 40°C$).

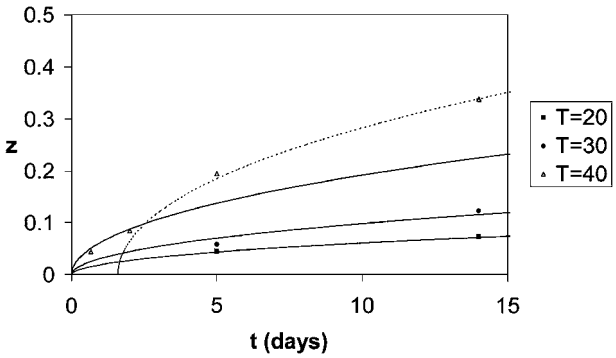

Figure 5 Fraction of mass dissolved z versus time [8] and fit (equations 31 and 32) for EFA solid spheres at $T = 20°C$, 30°C and 40°C (pOH = 0.3).

in time, and that at lower pOH (larger OH^- concentration) the removal is largest. Images of leached particles revealed the creation of a hollow structure originating from the leached glass phase with remains of needle shape inert (crystalline) material. This finding is in agreement with etching experiments [11, 12].

In Figs 3 and 4 the mass dissolved from cenospheres and solid spheres for EFA and LM, respectively, are depicted at pOH = 0.3 and 40°C. In Figs 5 and 6 the dissolution of solid spheres for EFA and LM, respectively, are set out for 20°C, 30°C and 40°C and at pOH = 0.3. One can see that cenospheres dissolve faster, and that higher temperature enhance the dissolution rate.

In the subsequent section a model is derived which adequately describes the dissolution experiments. The observation of a removed glass phase and an inert crystalline phase suggests the application of a shrinking core model [9, 13]. Furthermore, the trend of the dissolved mass versus time suggests a control by diffusion through the dissolved shell.

3. Dissolution model

In this section the dissolution of a spherical particle in an infinite reservoir of liquid is modelled. This particle is considered to have a phase that dissolves and leaves porosity, and an inert part that is unaffected. In fly ash and slag the dissolving part corresponds to the glass phase, whereas the inert part can be thought of as crystalline. The unreacted core shrinks, and the dissolved glass diffuses through the porous shell of inert material towards the solvent. Therefore, the part of the volume that is dissolving is named porosity ϕ and hence the inert part $1 - \phi$. This shrinking unreacted core model was first presented by Yagi and Kunii [9] and an extensive treatment can be found in Levenspiel [13]. Here, this model will be applied to the leaching of glass from fly ash assuming control by diffusion through the dissolved shell, following the treatment of Levenspiel [13]. The model presented here differs in two aspects from the conventional model:

1. Here we permit the sphere to be hollow, as is the case in cenospheres. From analyses by among others Pietersen [7, 8], Hemmings and Berry [12] it follows that some fly ash particles have a hollow core, which results in a lower mean density of these cenospheres. Some particles are really completely hollow, while other particles also contain material inside the hollow core (other solid and/or hollow particles). Here it is assumed that the outer enclosing wall will be sufficiently thick so that a breakthrough of this wall will not occur. Accordingly, the particle can be modelled as a completely hollow sphere.
2. From Figs 1–6 it follows that for glass removal rates up to about 20% the experiments follow a path which can be explained with a diffusion rate limited shrinking core model. For higher removal rates (appearing at higher OH^- concentrations and/or higher temperature), however, it seems that glass removal accelerates. Accordingly, here the sphere is considered to consist of two regions, the interior glass and the exterior glass, a concept, which is also mentioned by Hemmings and Berry [12].

Hence, consider a hollow spherical particle with an inner radius r_h and an outer radius R and an external surface area A. The particle possesses an outer and an inner region, the boundary between both regions designated as r_{i-o} and the reacting surface designated as r_c (Fig. 7). The time at which r_c reaches r_{i-o} is denoted as t_{i-o}.

In an alkali environment, OH^- ions are diffusing towards the reacting surface, whereas released glass ions (SiO_3^{2-} and others such as AlO_2^-) are diffusing from glass core to the surrounding liquid. Both SiO_2 and Al_2O_3 are the major constituents of the glass (Table I) and are hydrated to aforesaid ions for pH larger than about 12 [14, 15]. As the silica release has been measured by Pietersen [7, 8], here the release of this

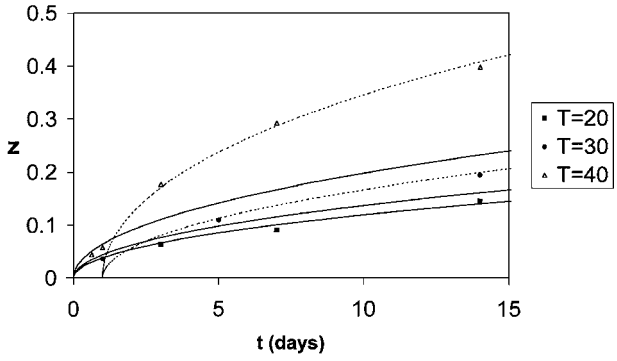

Figure 6 Fraction of mass dissolved z versus time [8] and fit (equations 31 and 32) for LM solid spheres at $T = 20°C$, 30°C and 40°C (pOH = 0.3).

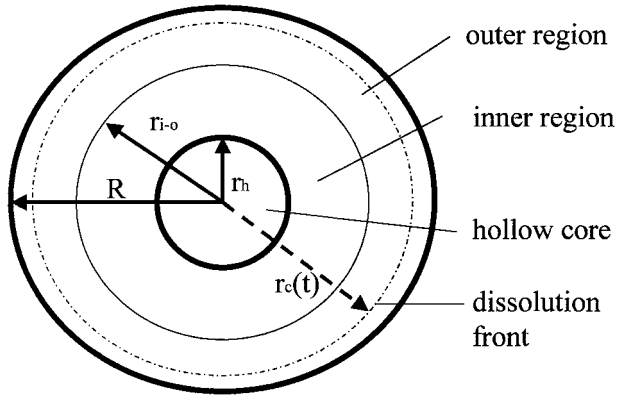

Figure 7 Schematic representation of dissolving hollow sphere containing two regions.

constituent is focused on. For all other constituents a similar analysis can be performed. Moreover, in Section 6. it will be reasoned that the dissolution process is governed indeed by the diffusion of the SiO_3^{2-} ion.

The steady-state diffusion equation for SiO_3^{2-} ion diffusing through the leached shell now reads:

$$\frac{\mathrm{d}\left(r^2 D_{eS}\dfrac{\mathrm{d}C_s}{\mathrm{d}r}\right)}{\mathrm{d}r} = 0 \tag{1}$$

The effective diffusion coefficient depends on the ion concentrations [16] and on the porosity of the leached shell [17]. When the concentration of one ion is smaller than the other, the effective diffusion coefficient takes the value of that ion present in smaller concentration [16]. Here it is assumed a priori that the concentration of the SiO_3^{2-} ion is much smaller than the OH^- concentration, so that D_e is constant. This assumption will be verified a posteriori. The effective diffusion coefficient in the porous shell is related to the bulk diffusion coefficient via Archie's law [17]:

$$D_{eS} = \phi^a D_S \tag{2}$$

The parameter a varies between 1.5 and 2.5, here a value of 2 is imposed, which is also recommended by Wakao and Smith [18]. The boundary conditions of Equation 1 read:

$$C_S(r = R) = 0 \tag{3}$$

$$C_S(r = r_c) = C_{Sc} \tag{4}$$

The first condition reflects the negligible small SiO_3^{2-} concentration in the surrounding liquid, whereas the second boundary condition states the SiO_3^{2-} concentration at the glass core.

Solving Equations 1, 3 and 4 yields

$$C_S(r) = \left[\frac{C_{Sc} r_c}{R - r_c}\right]\left[\frac{R}{r} - 1\right] \tag{5}$$

The SiO_3^{2-} molar flux from the glass surface now reads

$$\dot{m}_S = -D_{eS}\frac{\mathrm{d}C_S}{\mathrm{d}r}\bigg|_{r_c} = \frac{D_{eS} C_{Sc} R}{(R - r_c) r_c} \tag{6}$$

The silica decrease of the particle by dissolution now reads

$$\phi x_S \rho_g \frac{4\pi}{3}\frac{\mathrm{d}r_c^3}{\mathrm{d}t} = -A_c \dot{m}_S \tag{7}$$

in which ρ_g is the molar density of the glass and x_S its mole fraction of silica and whereby $\dot{m}_S$ follows from Equation 6. Inserting

$$A_c = 4\pi r_c^2 \tag{8}$$

and introducing

$$r^* = \frac{r}{R} \tag{9}$$

$$\tau = \frac{x_S \rho_g R^2}{6\phi D_S C_{Sc}} \tag{10}$$

in which Equation 2 has been substituted, yields the following first order ordinary differential equation for the dimensionless radius:

$$\frac{\mathrm{d}r_c^*}{\mathrm{d}t}\left(r_c^* - 1\right) r_c^* = \frac{1}{6\tau} \tag{11}$$

With as initial condition

$$r_c^*(t = 0) = 1 \tag{12}$$

in case the outer region is considered, and

$$r_c^*(t = t_{i-o}) = r_{i-o}^* \tag{13}$$

when the dissolution of the inner region is considered. Note that τ is different for the inner and outer regions, which are therefore denoted by τ_i and τ_o, respectively.

Integrating Equation 11 and application of Equations 12 and 13 yields, respectively:

$$t = \left(1 - 3r_c^{*2} + 2r_c^{*3}\right)\tau_o \tag{14}$$

$$t = \left(3r_{i-o}^{*2} - 2r_{i-o}^{*3} - 3r_c^{*2} + 2r_c^{*3}\right)\tau_i + t_{i-o} \tag{15}$$

which are both implicit relations of r^* as a function of time. Note that r_{i-o}^* and t_{i-o}, using Equation 14, are

related by:

$$t_{\mathrm{i-o}} = \left(1 - 3r_{\mathrm{i-o}}^{*2} + 2r_{\mathrm{i-o}}^{*3}\right)\tau_{\mathrm{o}} \tag{16}$$

Substituting this equation into Equation 15 produces:

$$t = \left(1 - 3r_{\mathrm{c}}^{*2} + 2r_{\mathrm{c}}^{*3}\right)\tau_{\mathrm{i}} + t_{\mathrm{i-o}}\left(1 - \frac{\tau_{\mathrm{i}}}{\tau_{\mathrm{o}}}\right) \tag{17}$$

for the inner region.

Here distinction has been made between an outer and inner region that may have among others different porosity (glass fraction), glass molar density and glass silica content. Often, also by Pietersen [7, 8], average values are given, such as the conversion factor. Hence, the expressions derived here will be related to average particle quantities.

The mean glass density of the particle is related to the properties of inner and outer region via

$$\overline{\phi\rho_{\mathrm{g}}}\left(R^3 - r_{\mathrm{h}}^3\right) = \phi_{\mathrm{o}}\rho_{\mathrm{go}}\left(R^3 - r_{\mathrm{i-o}}^3\right) + \phi_{\mathrm{i}}\rho_{\mathrm{gi}}\left(r_{\mathrm{i-o}}^3 - r_{\mathrm{h}}^3\right) \tag{18}$$

Similarly, the average glass silica content is related to the contents in outer and inner region via:

$$\overline{x_{\mathrm{S}}\phi\rho_{\mathrm{g}}}\left(R^3 - r_{\mathrm{h}}^3\right) = x_{\mathrm{So}}\phi_{\mathrm{o}}\rho_{\mathrm{go}}\left(R^3 - r_{\mathrm{i-o}}^3\right) + x_{\mathrm{Si}}\phi_{\mathrm{i}}\rho_{\mathrm{gi}}\left(r_{\mathrm{i-o}}^3 - r_{\mathrm{h}}^3\right) \tag{19}$$

The glass mass removed (or, conversion factor) for the outer region reads:

$$z = 1 - \frac{\phi_{\mathrm{o}}\rho_{\mathrm{go}}\left(r_{\mathrm{c}}^3 - r_{\mathrm{i-o}}^3\right) + \phi_{\mathrm{i}}\rho_{\mathrm{gi}}\left(r_{\mathrm{i-o}}^3 - r_{\mathrm{h}}^3\right)}{\overline{\phi\rho_{\mathrm{g}}}\left(R^3 - r_{\mathrm{h}}^3\right)} \tag{20}$$

Analogously, the fraction of glass silica dissolved (or, silica conversion factor) for the outer region follows from

$$z_{\mathrm{S}} = 1 - \frac{x_{\mathrm{So}}\phi_{\mathrm{o}}\rho_{\mathrm{go}}\left(r_{\mathrm{c}}^3 - r_{\mathrm{i-o}}^3\right) + x_{\mathrm{Si}}\phi_{\mathrm{i}}\rho_{\mathrm{gi}}\left(r_{\mathrm{i-o}}^3 - r_{\mathrm{h}}^3\right)}{\overline{x_{\mathrm{S}}\phi\rho_{\mathrm{g}}}\left(R^3 - r_{\mathrm{h}}^3\right)} \tag{21}$$

Combining Equations 18 and 20 and Equations 19 and 21 reveals

$$z_{\mathrm{S}} = z\frac{x_{\mathrm{So}}}{\overline{x_{\mathrm{S}}}} \tag{22}$$

The glass conversion rate of the inner region reads

$$z = 1 - \frac{\phi_{\mathrm{i}}\rho_{\mathrm{gi}}\left(r_{\mathrm{c}}^3 - r_{\mathrm{h}}^3\right)}{\overline{\phi\rho_{\mathrm{g}}}\left(R^3 - r_{\mathrm{h}}^3\right)} \tag{23}$$

and the silica conversion rate for the inner region is

$$z_{\mathrm{S}} = 1 - \frac{x_{\mathrm{Si}}\phi_{\mathrm{i}}\rho_{\mathrm{gi}}\left(r_{\mathrm{c}}^3 - r_{\mathrm{h}}^3\right)}{\overline{x_{\mathrm{S}}\phi\rho_{\mathrm{g}}}\left(R^3 - r_{\mathrm{h}}^3\right)} \tag{24}$$

Combining Equations 23 and 24 reveals that for the inner region holds:

$$1 - z_{\mathrm{S}} = (1 - z)\frac{x_{\mathrm{Si}}}{\overline{x_{\mathrm{S}}}} \tag{25}$$

Note that Equation 20 coincides with Equation 23 and Equation 22 with Equation 24 for $r_{\mathrm{c}} = r_{\mathrm{i-o}}$ (i.e. on the transition of inner and outer region), as would be expected.

In order to express r_{c} into z and z_{S}, Equation 21 is rewritten by inserting Equation 19 in the nominator and introducing b (which can be seen as is the ratio between apparent mean density of the hollow sphere and the mean glass density):

$$b = \frac{\rho_{\mathrm{a}}}{\rho_{\mathrm{g}}} = 1 - \frac{r_{\mathrm{h}}^3}{R^3} = 1 - r_{\mathrm{h}}^{*3} \tag{26}$$

yielding for the outer region:

$$r_{\mathrm{c}}^{*3} = 1 - z_{\mathrm{S}}b\frac{\overline{x_{\mathrm{S}}\phi\rho_{\mathrm{g}}}}{x_{\mathrm{So}}\phi_{\mathrm{o}}\rho_{\mathrm{go}}} = 1 - zb\frac{\overline{\phi\rho_{\mathrm{g}}}}{\phi_{\mathrm{o}}\rho_{\mathrm{go}}} \tag{27}$$

see Equations 9 and 22. Substituting Equations 19 and 26 into Equation 23 yields for the inner region

$$\begin{aligned} r_{\mathrm{c}}^{*3} &= 1 - b + (1 - z_{\mathrm{S}})b\frac{\overline{x_{\mathrm{S}}\phi\rho_{\mathrm{g}}}}{x_{\mathrm{Si}}\phi_{\mathrm{i}}\rho_{\mathrm{gi}}} \\ &= 1 - b + (1 - z)b\frac{\overline{\phi\rho_{\mathrm{g}}}}{\phi_{\mathrm{i}}\rho_{\mathrm{gi}}} \end{aligned} \tag{28}$$

see Equations 9 and 25. Equations 27 and 28 can be combined with Equations 14 and 17, respectively, yielding

$$t = \left(1 - 3\left(1 - z_{\mathrm{S}}b\frac{\overline{x_{\mathrm{S}}\phi\rho_{\mathrm{g}}}}{x_{\mathrm{So}}\phi_{\mathrm{o}}\rho_{\mathrm{go}}}\right)^{\frac{2}{3}} + 2\left(1 - z_{\mathrm{S}}b\frac{\overline{x_{\mathrm{S}}\phi\rho_{\mathrm{g}}}}{x_{\mathrm{So}}\phi_{\mathrm{o}}\rho_{\mathrm{go}}}\right)\right)\tau_{\mathrm{o}} \tag{29}$$

$$t = \left(1 - 3\left(1 - b + (1 - z_{\mathrm{S}})b\frac{\overline{x_{\mathrm{S}}\phi\rho_{\mathrm{g}}}}{x_{\mathrm{Si}}\phi_{\mathrm{i}}\rho_{\mathrm{gi}}}\right)^{\frac{2}{3}} + 2\left(1 - b + (1 - z_{\mathrm{S}})b\frac{\overline{x_{\mathrm{S}}\phi\rho_{\mathrm{g}}}}{x_{\mathrm{Si}}\phi_{\mathrm{i}}\rho_{\mathrm{gi}}}\right)\right)\tau_{\mathrm{i}} + t_{\mathrm{i-o}}\left(1 - \frac{\tau_{\mathrm{i}}}{\tau_{\mathrm{o}}}\right) \tag{30}$$

Note that Equations 27 and 28 become identical when the spheres are homogeneous, i.e. when $\overline{x_{\mathrm{S}}\phi\rho_{\mathrm{g}}} = x_{\mathrm{So}}\phi_{\mathrm{o}}\rho_{\mathrm{go}} = x_{\mathrm{Si}}\phi_{\mathrm{i}}\rho_{\mathrm{gi}}$, and that Equations 29 and 30 than reduce to

$$t = \left(1 - 3(1 - zb)^{\frac{2}{3}} + 2(1 - zb)\right)\tau_{\mathrm{o}} \tag{31}$$

$$t = \left(1 - 3(1 - zb)^{\frac{2}{3}} + 2(1 - zb)\right)\tau_{\mathrm{i}} + t_{\mathrm{i-o}}\left(1 - \frac{\tau_{\mathrm{i}}}{\tau_{\mathrm{o}}}\right) \tag{32}$$

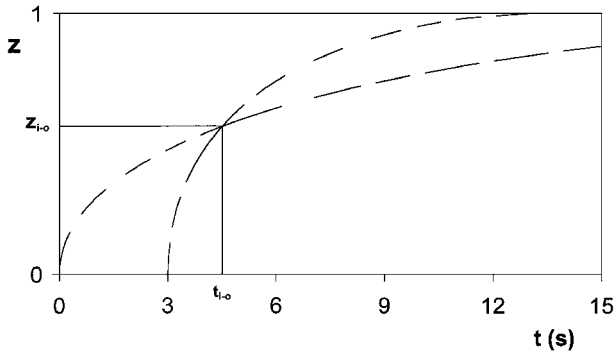

(a)

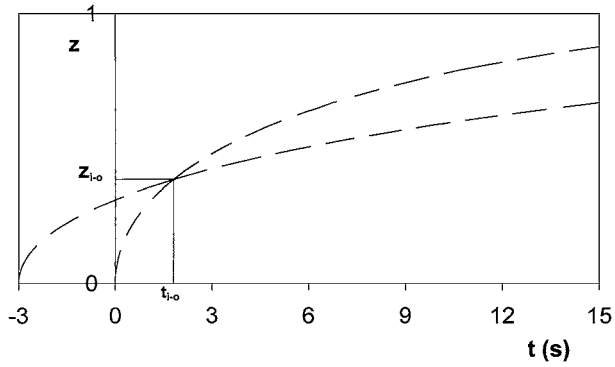

(b)

Figure 8 (a) Mass removal versus time for a solid sphere ($b = 1$) using Equations 31 and 32, $\tau_o = 30$ s., $\tau_i = 10$ s. and $t_{i-o}\,(1-\tau_i/\tau_o) = 3$ s; (b) Mass removal versus time for a solid sphere ($b = 1$) using Equations 31 and 32, $\tau_o = 30$ s., $\tau_i = 80$ s. and $t_{i-o}\,(1-\tau_i/\tau_o) = -3$ s.

Furthermore, note that for $\tau_i = \tau_o$ (see Equation 10), Equations 31 and 32 are identical, in case of solid spheres ($b = 1$) they then reduce to the common shrinking core model expressions.

In Fig. 8a z is depicted against t for $b = 1$ (massive spheres) using Equations 31 and 32. As example, τ_o has been set equal to 30 s., τ_i to 10 s. and $t_{i-o}(1-\tau_i/\tau_o)$ to 3 s., i.e. a case whereby the inner region is more reactive than the outer region.

One can readily see that for $\tau_i < \tau_o$ the glass removal line crosses the horizontal axis at $t > 0$ and climbs steeper in time. This behaviour was also seen in Figs 1–6, implying two regions with two different τ. In the following section Equations 31 and 32 are applied to the experimental data depicted in said Figures. In Fig. 8b a case whereby the inner region is less reactive than the outer region is depicted, τ_o has been set equal to 30 s., τ_i to 80 s. and $t_{i-o}\,(1-\tau_i/\tau_o)$ to -3 s. One can see that when the inner region is attained, removal proceeds slower.

4. Model application

In Figs 1–6 Equation 31 has been fitted to the experimental data by adapting τ_0. For the solid spheres b has been set equal to unity, wheras for the cenospheres b equals 0.5 [7, 8]. Furthermore, it has been assumed a priori that the silica is homogeneously distributed, i.e. $\overline{x_S \phi \rho_g} = x_{so}\phi_o\rho_{go} = x_{Si}\phi_i\rho_{gi}$ and hence, $z = z_S$ (the fraction of removed glass is identical to fraction of removed silica, this latter quantity was measured by Pietersen [7, 8]). When the inner region has been reached, i.e. when Equation 31 is not able to match the measured removal rates anymore (at larger t), Equation 32 was fitted to these data by adapting τ_i.

From Figs 1–6 it follows that for the solid spheres the inner region is attained when about 7% (LM) to 9% (EFA) of the silica/glass has been dissolved ($= z_{i-o} = z_{Si-o}$). Said values imply that the boundary between both regions is located at about 96–97% of the external radius of the sphere. These values are identical for all experiments, regardless the pOH and temperature of the experiment. At higher pH and higher temperature the lines intersect after 1–2 days ($= t_{i-o}$), whereas for low temperatures even after 15 days the—more reactive—inner region has not been attained yet. For the cenospheres, Figs 3 and 4 learn that the outer region comprises 12% (EFA) to 13% (LM) of sphere mass. As $b = 0.5$ (and hence $r_h^{*3} = 0.80$, see Equation 26), i.e. the inner core mass of cenospheres is effectively reduced by about 50% in comparison to solid spheres, it can be concluded that the thickness of the outer layer of hollow spheres is the same (for LM) or a little thinner (EFA) than for their solid counterparts, and amounts about 2 μm as $d = 38$–50 μm. Note that this outer hull comprises about half of the thickness of the cenosphere wall: $0.2 \times (38$–$50\ \mu\text{m})/2 = 3.8$–$5\ \mu$m.

For each set of experimental data the best τ has been chosen at first sight. In Tables II–VII the assessed values of τ have been listed for all experiments. One can see that the reaction time τ decreases, i.e. increasing

TABLE II Reaction time τ for various pOH and [OH$^-$] for EFA solid spheres ($T = 40$°C) assuming $\overline{x_S}/x_{Si} = 1$ and $\overline{x_S}/x_{So} = 1$

pOH	[OH$^-$] (mole/l)	τ_o (days)	τ_i (days)	$t_{i-o}(1-\tau_i/\tau_o)$ (days)
1.0	0.100	3500		
0.6	0.251	1200		
0.3	0.501	750	275	1.6

TABLE III Reaction time τ for various pOH and [OH$^-$] for LM solid spheres ($T = 40$°C) assuming $\overline{x_S}/x_{Si} = 1$ and $\overline{x_S}/x_{So} = 1$

pOH	[OH$^-$] (mole/l)	τ_o (days)	τ_i (days)	$t_{i-o}(1-\tau_i/\tau_o)$ (days)
1.0	0.100	2500		
0.6	0.251	1200	550	1.3
0.3	0.501	700	190	1.0

TABLE IV Reaction time τ for EFA cenospheres and solid spheres (pOH = 0.3, $T = 40$°C) assuming $\overline{x_S}/x_{Si} = 1$ and $\overline{x_S}/x_{So} = 1$

Sphere	τ_o (days)	τ_i (days)	$t_{i-o}(1-\tau_i/\tau_o)$ (days)
Ceno	1000	180	1.1
Solid	750	275	1.6

TABLE V Reaction time τ for LM cenospheres and solid spheres (pOH = 0.3, $T = 40$°C) assuming $\overline{x_S}/x_{Si} = 1$ and $\overline{x_S}/x_{So} = 1$

Sphere	τ_o (days)	τ_i (days)	$t_{i-o}(1-\tau_i/\tau_o)$ (days)
Ceno	900	190	1.2
Solid	700	190	1.0

TABLE VI Reaction time τ for EFA solid spheres for various temperatures (pOH = 0.3) assuming $\overline{x_S}/x_{Si} = 1$ and $\overline{x_S}/x_{So} = 1$

T (K)	τ_o (days)	τ_i (days)	$t_{i-o}(1-\tau_i/\tau_o)$ (days)	K_o (l/mole)	ΔG_o (J/mole)
293	8000			4.46×10^{-17}	9.1717×10^4
303	3000			2.84×10^{-16}	9.0179×10^4
313	750	275	1.6	4.02×10^{-15}	8.6264×10^4
ΔH (J/mole)				1.80×10^5	
ΔS (J/mole K)				298	
ΔG_{298} (J/mole)				9.120×10^4	

TABLE VII Reaction time τ for LM solid spheres for various temperatures (pOH = 0.3) assuming $\overline{x_S}/x_{Si} = 1$ and $\overline{x_S}/x_{So} = 1$

T (K)	τ_o (days)	τ_i (days)	$t_{i-o}(1-\tau_i/\tau_o)$ (days)	K_o (l/mole)	ΔG_o (J/mole)	K_i (1/mole)	ΔG_i (J/mole)
293	2000			8.99×10^{-14}	7.3181×10^4		
303	1500	900	1.0	1.40×10^{-13}	7.4563×10^4	3.41×10^{-13}	7.2322×10^4
313	700	190	1.0	4.99×10^{-13}	7.3716×10^4	4.84×10^{-12}	6.7805×10^4
ΔH (J/mole)				8.00×10^4		1.90×10^5	
ΔS (J/mole K)				19		390	
ΔG_{298} (J/mole)				7.434×10^4		7.378×10^4	

reactivity, with increasing hydroxide concentration and temperature (Tables II, III, VI and VII).

Moreover, the inner region appears to be more reactive that the outer region ($\tau_i < \tau_o$). Both for the ceno and solid spheres of both LM and EFA fly ash and for all temperatures and pOH, the reactivity of the inner region is about 2–5 times the reactivity of the outer region (Tables IV and V). Moreover, it seems that for the LM fly ash the inner region of both ceno and solid spheres have the same reactivity. For both EFA and LM fly ash the outer region of cenospheres is less reactive than the outer region of solid spheres.

In order to investigate the dependence of τ against the hydroxide content, in Tables II and III also $[OH^-]$ has been included, which directly follows from the pOH. Subsequently, in Figs 9 and 10, τ^{-1} has been set out against $[OH^-]$ pertaining to the outer region of EFA and LM, respectively. For LM (Fig. 10) also τ^{-1} has been set out for the inner region, as two values are listed in Table III.

From both Figures one might conclude that, τ for the outer region depends linearly on $[OH^-]$, or is a power of $[OH^-]$. Accordingly, the following function has been fitted in through the inner and out region τ^{-1} (Figs 9 and 10):

$$\tau^{-1} = c[OH^-]^a \tag{33}$$

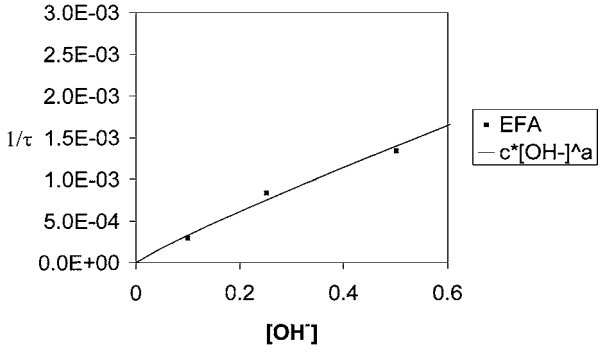

Figure 9 Reaction time τ against $[OH^-]$ for EFA solid spheres ($T = 40°C$), outer region only.

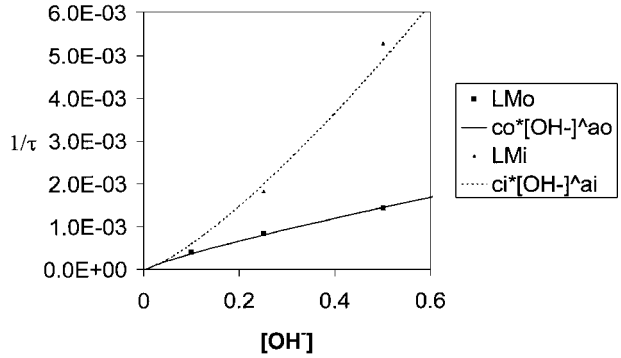

Figure 10 Reaction time τ against $[OH^-]$ for LM solid spheres ($T = 40°C$), inner and outer region.

with $c = 0.0026$ (mole/l)$^{-a}$s^{-1} and $a = 0.9$ (EFA outer region), $c = 0.0030$ (mole/l)$^{-a}$s^{-1} and $a = 1$ (LM outer region) and $c = 0.0140$ (mole/l)$^{-a}$s^{-1} and $a = 1.4$ (LM inner region).

The dissolution process seems to have a direct and positive relation with $[OH^-]$. Song and Jennings [5] found a similar dependence for dissolution of slags: their measured dissolution was proportional to 10^{apH} (with a ranging from 0.97 to 1.60), which corresponds to Equation 33. Slags contain the same glass components as fly ashes, but usually in different quantities (slags are usually richer in CaO). In the next section a brief chemical explanation is presented which will support the experimental findings of this section.

5. Chemical analysis

From the composition of the fly ashes as presented in Table I it is clear that the glass phases of both fly ashes consist of SiO_2, as well as the networkformers Al_2O_3, Fe_2O_3, TiO_2 and P_2O_5, and the network modifiers CaO, MgO, Na_2O and K_2O [12].

In Pourbaix [19] the prevailing equilibria of the various substances can be found for pH > 12 and an electric potential ranging from −0.3 to 0.2 V, values that are found in ordinary Portland and slag cement systems

[20]. Paul [14, 15] also presented hydration reactions for SiO_2, Al_2O_3, Na_2O and K_2O. Accordingly, from all this literature it follows that for pH > 12 vitreous silica is hydrated as

$$SiO_2 + 2OH^- \Leftrightarrow SiO_3^{2-} + H_2O \tag{34}$$

and that Al_2O_3 is hydrated according to

$$Al_2O_3 + 2OH^- \Leftrightarrow 2AlO_2^- + H_2O \tag{35}$$

that CaO reacts as follows

$$CaO + H_2O \Leftrightarrow Ca^{2+} + 2OH^- \tag{36}$$

that Na_2O reacts as follows

$$Na_2O + H_2O \Leftrightarrow 2Na^+ + 2OH^- \tag{37}$$

that Fe_2O_3 reacts as follows

$$Fe_2O_3 + 3H_2O \Leftrightarrow 2Fe^{3+} + 6OH^- \tag{38}$$

and that TiO_2 hydrates as follows

$$TiO_2 + OH^- \Leftrightarrow HTiO_3^- \tag{39}$$

Accordingly, the following reaction of the fly ash glass is proposed as

$$\begin{aligned} &SiO_2 \cdot \alpha Al_2O_3 \cdot \beta CaO \cdot \gamma Na_2O \cdot \delta Fe_2O_3 \cdot \varepsilon TiO_2 \\ &\quad + (\beta + \gamma + 3\delta)H_2O + (2 + 2\alpha + \varepsilon)OH^- \Leftrightarrow SiO_3^{2-} \\ &\quad + 2\alpha AlO_2^- + \beta Ca^{2+} + 2\gamma Na^+ + 2\delta Fe^{3+} \\ &\quad + \varepsilon HTiO_3^- + (1 + \alpha)H_2O + 2(\beta + \gamma + 3\delta)OH^- \end{aligned} \tag{40}$$

Note that silica, aluminium oxide and titanium oxide consume hydroxides, whereas the earth alkalis (CaO, MgO), alkalis (Na_2O, K_2O) and iron oxide produce them. As slag contain the same components as fly ashes, it is believed that the model might be applicable to the dissolution of this material as well. In case a fly ash or a slag also contains MnO and SO_3, the former reacts as CaO/MgO (to Mn^{2+}), and the latter likewise SiO_2 (to SO_4^{2-}).

As the activity of pure liquids and solids are unity, the reaction product is defined as

$$K = \frac{[AlO_2^-]^{2\alpha}[Ca^{2+}]^{\beta}[Na^+]^{2\gamma}[Fe^{3+}]^{2\delta}[HTiO_3^-]^{\varepsilon}[SiO_3^{2-}]}{[OH^-]^{2+2\alpha-2\beta-2\gamma-6\delta+\varepsilon}} \tag{41}$$

Invoking $[AlO_2^-] = 2\alpha\ [SiO_3^{2-}]$, $[Ca^{2+}] = \beta\ [SiO_3^{2-}]$, $[Na^+] = 2\gamma\ [SiO_3^{2-}]$, $[Fe^{3+}] = 2\delta\ [SiO_3^{2-}]$ and $[HTiO_3^-] = \varepsilon\ [SiO_3^{2-}]$ yields

$$\left[SiO_3^{2-}\right] = \left(\frac{K}{(2\alpha)^{2\alpha}\beta^{\beta}(2\gamma)^{2\gamma}(2\delta)^{2\delta}\varepsilon^{\varepsilon}}\right)^{\frac{1}{1+2\alpha+\beta+2\gamma+2\delta+\varepsilon}} [OH^-]^a \tag{42}$$

with

$$a = \frac{2 + 2\alpha - 2\beta - 2\gamma - 6\delta + \varepsilon}{1 + 2\alpha + \beta + 2\gamma + 2\delta + \varepsilon} \tag{43}$$

Note that the powers appearing in the denominator of the first factor of Equation 42, $(2\alpha)^{2\alpha}$ etc., are of order unity. The function x^x namely attains a value of 1 at $x = 0$ and $x = 1$, and has a minimum of $(1/e)^{(1/e)}$ (≈ 0.69) at $x = e^{-1}$. From Table VIII it can be seen that the values of α etc. are such that 2α etc. all fall in the range 0 to 1, so that $(2\alpha)^{2\alpha}$ etc. all have a value between 0.69 and 1. Furthermore, it will be demonstrated that K is (much) smaller than unity. So, with increasing α etc. (i.e. less silica) the power of the first factor decreases, and hence, the factor increases. Accordingly, when the silica content diminishes, the solubility (reactivity) is enhanced. This trend is also supported by the second factor on the right-hand side of Equation 42. The power a decreases with increasing α, β etc., see Equation 43. For β, γ and δ this effect is obvious. But this trend also holds for α and ε: the function $(2 + x)/(1 + x)$ attains a value of 2 at $x = 0$, and monotonically decreases towards the asymptotic value of 1 for large x. Considering that $[OH^-]$ is usually smaller than 1 mole/1, increasing α, β etc. imply a smaller a and a larger second factor in Equation 42, i.e. the same trend as the first factor.

Considering the equilibrium product it follows that the hydration of pure silica is quadratically dependent on $[OH^-]$ ($\alpha = \beta = \gamma = \delta = \varepsilon = 0$). In case of a pure aluminosilicate glass ($\beta = \gamma = \delta = \varepsilon = 0$), the power a is located between unity and 2, but depending weakly on changes in α. E.g., for α ranging from 1/4 to 1, this power ranges from 1.66 to 1.33 (it equals 1.5 for $\alpha = 0.5$). For a alkali silicate glasses ($\alpha = \beta = \delta = \varepsilon = 0$), it follows from Equation 43 that the power a is smaller than unity when $\gamma > 0.25$.

In Table VIII the mass fraction of all glass phases in the studied fly ashes are listed, based on the data of Table I. For vitreous SiO_2 and Al_2O_3 they follow from the total mass fraction of each substance minus the crystalline SiO_2 (in quartz and in mullite) and crystalline Al_2O_3 (in mullite only), see Table I, respectively. Using these mass fractions, the mean mole fraction of all components in the glass can be computed using the molecular mass of each component, which are included in Table VIII for the EFA and LM solid spheres only (between the brackets). With these mole fractions subsequently the mean α, β, γ, δ and ε and a can be computed for solid EFA and LM, which are included in Table VIII as well. For this calculation it is assumed MgO to react as CaO and K_2O as $Na_2O \cdot P_2O_5$ can be neglected, as its presence is minor (Tables I and VIII).

TABLE VIII Mass and mole fraction (between brackets) of the glass phases in LM and EFA spheres. Mass fraction is based on total fly ash mass, mole fraction is based on glass phase only

	EFA		LM		M
	Solid ($\bar{x}$)	Ceno	Solid ($\bar{x}$)	Ceno	(g/mole)
Crystalline					
$SiO_2 + Al_2O_3$	5.1%	8.4%	33.3%	37.8%	
Glass					
SiO_2	51.96% (0.648)	47.05%	38.79% (0.695)	40.41%	60
Al_2O_3	25.89% (0.190)	28.06%	16.48% (0.174)	13.54%	102
Fe_2O_3	4.65% (0.022)	2.96%	3.50% (0.024)	2.02%	160
P_2O_5	n.d.	n.d.	0.54% (0.004)	n.d.	142
TiO_2	1.20% (0.011)	0.91%	1.90% (0.026)	1.43%	80
CaO	2.83% (0.038)	0.80%	2.75% (0.053)	1.15%	56
MgO	1.82% (0.034)	1.41%	0.28% (0.008)	0.24%	40
Na_2O	1.84% (0.022)	1.94%	0.37% (0.006)	0.38%	62
K_2O	4.40% (0.035)	5.68%	1.00% (0.011)	1.02%	94
$\bar{\alpha}(=\bar{x}_A/\bar{x}_S)$	0.293		0.250		
$\bar{\beta}(=(\bar{x}_C+\bar{x}_M)/\bar{x}_S)$	0.111		0.087		
$\bar{\gamma}(=(\bar{x}_N+\bar{x}_K)/\bar{x}_S)$	0.088		0.026		
$\bar{\delta}(=\bar{x}_F/\bar{x}_S)$	0.034		0.034		
$\bar{\varepsilon}(=\bar{x}_T/\bar{x}_S)$	0.017		0.037		
$\bar{a}$ (Equation 43)	1.022		1.208		
$\bar{M}$	71		72		

One can readily see that the power a takes a value of 1.022 (EFA) and 1.208 (LM), which is not in line with the fitted power of the previous section (1.4 in LM inner region, 0.9 and 1 in EFA and LM outer region, respectively). This deviation can probably be attributed to the inhomogeneity of the fly ash, as will be reasoned in more detail in the following section.

6. Effect of inhomogeneity

Pietersen [7, 8] has measured that the release of SiO_2, Al_2O_3, and K_2O is virtually congruent. The release of other constituents was, however, not measured. Moreover, experiments by Dudas and Warren (1987) reveal that the glass components K_2O, Na_2O, CaO, MgO, and Fe_2O_3 are concentrated in the exterior (outer) hull. Smith [21] found a similar enrichment in the outer layer, and explained this inhomogeneity by the fact that the boiling point of silica and aluminiumoxide are practically the same (2950°C and 2980°C, respectively), and higher than the boiling points of all other components. This will result in a concentration of more volatile components (i.e. the other oxides) in the outer layer.

In a previous section it was found that for the solid LM spheres the power a is higher in outer region (0.9) than in inner region (1.4), also implying higher values of β, γ etc. in outer region (see Eq. 43). To explore the effect of a inhomogeneous composition, the silica, aluminiumoxide, alkalis, earth alkalis etc. are redistributed: the outer region is enriched with the (minor) constituents K_2O, Na_2O, CaO, MgO, Fe_2O_3 and TiO_2. The molar ratio of the major components aluminiumoxide and silica is not altered: $\alpha_i = \alpha_o = \bar{\alpha}$. However, the redistribution of the other components has to obey the mass balance of each component. Assuming the spheres to have a constant glass molar density ($\overline{\phi\rho_g} = \phi_o\rho_{go} = \phi_i\rho_{gi}$ and applying Equation 19 to $x_C + x_M(=\beta x_S)$ and inserting $r_h = 0$ (solid sphere) yields:

$$\bar{\beta} = \beta_o\left(1 - r_{i-o}^{*3}\right)\frac{x_{So}}{\overline{x_S}} + \beta_i r_{i-o}^{*3}\frac{x_{Si}}{\overline{x_S}}$$
$$= \beta_o z_{Si-o} + \beta_i(1 - z_{Si-o}) \qquad (44)$$

see Equations 27 and 28, whereby $z_{Si-o} = 7\%$ (volume fraction outer region, see Section 4.). Similar equations hold for γ, δ and ε. As example values for β_i, β_o, γ_i γ_o etc. are given in Table IX that obey Equation 44.

As can been seen from this table, as example, the values in outer region are enriched by a factor of about 2 in comparison with the mean values. In Table IX also the pertaining a of inner and outer region (a_i and a_o) have been included. The values of a_i and a_o that follow from the redistribution of the minor constituents indeed approach the values of a_i and a_o that have been found in the previous section.

Following the redistribution, the silica (and aluminiumoxide) is concentrated in the inner region. Consequently, Equations 29 and 30 need to be fit again through the experiments, but now taking into account that $\overline{x_S}/x_{Si}$ and $\overline{x_S}/x_{So}$ are not equal to unity. By definition, the mole fraction of silica is related to α, β, γ, δ and ε via

$$(\alpha + \beta + \gamma + \delta + \varepsilon + 1)x_S = 1 \qquad (45)$$

TABLE IX Mean composition of LM solid spheres and redistribution of phases in inner and outer region

	Mean value (Table VIII)	Inner region	Outer region
α	0.250	0.250	0.250
β	0.087	0.080	0.174
γ	0.026	0.024	0.052
δ	0.034	0.031	0.068
ε	0.037	0.034	0.074
a (Equation 43)	1.208	1.238	0.862

and therefore

$$\frac{\overline{x_S}}{x_{So}} = \frac{\bar{\alpha} + \beta_o + \gamma_o + \delta_o + \varepsilon_o + 1}{\bar{\alpha} + \bar{\beta} + \bar{\gamma} + \bar{\delta} + \bar{\varepsilon} + 1} \quad (46)$$

$$\frac{\overline{x_S}}{x_{Si}} = \frac{\bar{\alpha} + \beta_i + \gamma_i + \delta_i + \varepsilon_i + 1}{\bar{\alpha} + \bar{\beta} + \bar{\gamma} + \bar{\delta} + \bar{\varepsilon} + 1} \quad (47)$$

yielding $x_{Si}/\overline{x_S} = 1.010$ and $x_{So}/\overline{x_S} = 0.886$. So, by the redistribution the silica concentration is reduced by 11% in the outer hull, whereas it is enlarged by about 1% in the inner region (relative to the average mole fraction). With said values Equations 29 and 30 are fitted again for the LM solid sphere experiments as depicted in Figs 2 and 6, yielding new values of τ_o and τ_i, which are included in Tables X and XI.

Comparing the newly determined τ_o and τ_i in Tables X and XI with the values in Tables III and VII, respectively, reveal that the τ_i are the same. This is no surprise as $\overline{x_S}/x_{Si}$ is close to unity so that the fitted lines have the same form. On the other hand, for the outer region all newly fitted τ_o are about 15% smaller than the fit with $x_{So} = \overline{x_S}$. Note that x_s appears in τ (Equation 10, and that for the first fit it corresponds to $\overline{x_S}$, and the second fit to x_{so} (which is about 13% smaller than $\overline{x_S}$ due to the redistribution). Consequently, fitting based on mean particle composition ($\overline{x_S}/x_{So} = 1$, resulting in Tables III and VII) and based on different inner an outer composition ($\overline{x_S}/x_{So} = 1.128$, resulting in Tables IX and X), yields practically the same C_{Sc} (as R, ϕ, ρ_g and D_S are constant).

7. Thermodynamic analysis

On the basis of the experimental data and the proposed reaction mechanism in the previous section, thermodynamic data for the fly ash can be determined. The first step in this analysis is the determination of K that appears in Equations 41 and 42.

It is expected that the dissolution process to be governed by the ion that diffuses the slowest. Here, only the diffusion coefficients of $[AlO_2^-]$ and $[SiO_3^{2-}]$ are compared, which are not both directly available. Accordingly, D_A^0 was estimated using the diffusion coefficients of the similar ions NO_2^- (1.912×10^{-9} m^2/s) and ClO_2^- (1.385×10^{-9} m^2/s), yielding $D_A^0 = 1.7 \times 10^{-9}$ m^2/s at $T = 298$ K [22]. Similarly, D_S^0 was estimated using the diffusion coefficients of CO_3^{2-} (0.912×10^{-9} m^2/s) and SO_3^{2-} (1.064×10^{-9} m^2/s), yielding $D_S^0 = 1.0 \times 10^{-9}$ m^2/s at $T = 298$ K [22]. Note that the molecular mass of aluminium lies between the molecular masses of nitrogen and chloride, and silicon between carbon and sulphur, so that the estimation is expected to a yield reasonable result. As D_A (but also the diffusion coefficients of Ca^{2+}, Na^+, K^+ and Fe^{3+} [22]) is larger than D_S, it is believed henceforth that the process is governed by the diffusion of SiO_3^{2-} and hence, $D_S C_{sc}$ appearing in Equation 10 to correspond to $D_S[SiO_3^{2-}]$. For deviating temperatures, D_S is determined via

$$D_S = \frac{T}{298\ \text{K}} D_S^0 \quad (48)$$

Combining Equations 10, 42 and 48 yields

$$K = (2\alpha)^\alpha (\beta)^\beta (2\gamma)^{2\gamma} (2\delta)^{2\delta} (\varepsilon)^\varepsilon \times \left[\frac{x_S \rho_g R^2}{6\phi D_S^0 \tau} \frac{298\ \text{K}}{T}\right]^{1+2\alpha+\beta+2\gamma+2\delta+\varepsilon} \times [OH^-]^{-2-2\alpha+2\beta+2\gamma+6\delta-\varepsilon} \quad (49)$$

The physical properties that appear in this equation are known: R (22 μm), ϕ (Table I), while ρ_g follows from the density (about 2450 kg/m^3) divided by the mean molar mass. The mean molar mass of the glass follows from the sum of the molar fraction of each constituent times its molar mass ($\bar{M} = \Sigma x_k M_k$), which are included in Table VIII as well. The τ at various temperature have been determined in the previous sections and are listed in Tables VI, VII and XI, as well as $[OH^-]$ and the temperature.

Using the data of Tables VI and VII, the K of EFA and LM solid spheres, respectively, are computed using Equation 49 and the result is included in both tables as well. For inner and outer region K is denoted by K_i and K_o, respectively. For these computations the mean values of α, β etc. and $\overline{x_S}$ have been used. Using the data of Table XI, K of LM solid spheres are computed using Equation 49 and the result is included in this table as well. For these computations the prevailing values of outer (β_o, γ_o, δ_o, ε_0 and x_{So}) and inner region (β_i, γ_i, δ_i, ε_i and x_{Si}) have been used.

The three tables indicate that K increases with temperature, implying improved dissolution/reaction with

TABLE X Reaction time τ for various pOH and $[OH^-]$ for LM solid spheres ($T = 40$°C) based on $\overline{x_S}/x_{Si} = 0.990$ and $\overline{x_S}/x_{So} = 1.128$

pOH	$[OH^-]$ (mole/l)	τ_o (days)	τ_i (days)	$t_{i-o}(1 - \tau_i/\tau_o)$ (days)
1.0	0.100	2100		
0.6	0.251	1000	550	1.3
0.3	0.501	600	190	1.0

TABLE XI Reaction time τ for LM solid spheres for various temperatures (pOH = 0.3) based on $\overline{x_S}/x_{Si} = 0.990$ and $\overline{x_S}/x_{So} = 1.128$

T (K)	τ_o (days)	τ_i (days)	$t_{i-o}(1 - \tau_i/\tau_o)$ (days)	K_o (l/mole)	ΔG_o (J/mole)	K_i (l/mole)	ΔG_i (J/mole)
293	1800			3.46×10^{-16}	8.6724×10^4		
303	1300	900	1.0	6.19×10^{-16}	8.8222×10^4	2.97×10^{-13}	7.2670×10^4
313	650	190	1.0	2.30×10^{-15}	8.7715×10^4	4.10×10^{-12}	6.8235×10^4
ΔH (J/mole)					9.20×10^4		1.81×10^5
ΔS (J/mole K)					15		359
ΔG_{298} (J/mole)					8.753×10^4		7.402×10^4

increasing temperature. Furthermore, the values of K and Equation 42 confirm that $[SiO_3^{2-}]$ is much smaller than $[OH^-]$ indeed, so that the assumption of constant D_e is valid (Section 3). With these K one can determine the standard free energy of reaction ΔG by

$$K = e^{\frac{-\Delta G}{RT}} \tag{50}$$

ΔG is the sum of free energies of formation of the products in their standard states minus the free energies of formation of the reactants in their standard states [14, 15], Babushkin *et al.* [23]. In Tables VI, VII and XI the resulting ΔG are included using $R = 8.31439$ J/mole K.

The connection of ΔG with enthalpy and entropy of reaction is

$$\Delta G = \Delta H - T\Delta S \tag{51}$$

in which ΔH and ΔS are the sum of standard heats of formation and of the standard entropies, respectively, where each sum is constituted by the sum of the products minus the sum of the reactants. In order to specify ΔH and ΔS, $-R$ Ln (K) has been set out against $1/T$ for LM and EFA in Fig. 11, taking the values of Tables VI and VII and in Fig. 12, taking the values of Table X. A straight line has been fitted through the experimental values, whereby

$$-R\ \mathrm{Ln}(K) = \frac{\Delta H}{T} - \Delta S \tag{52}$$

see Equations 50 and 51. The fitted values of ΔH and ΔS have been included in Tables VI, VII and XI. Next, with the standard free energy of reaction ΔG, one is

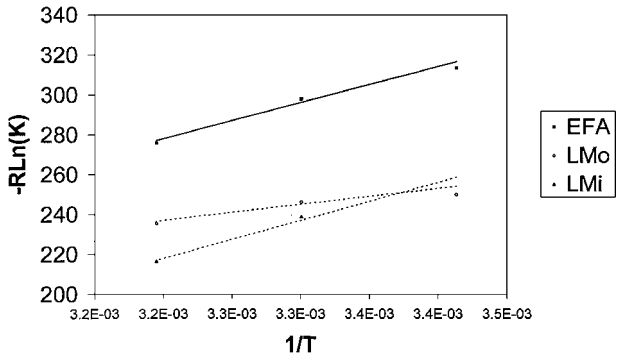

Figure 11 $-R$ Ln K versus $1/T$ for LM (inner and outer region) and EFA (outer region only) solid fly ash, based on $\overline{x_S}/x_{Si} = 1$ and $\overline{x_S}/x_{So} = 1$.

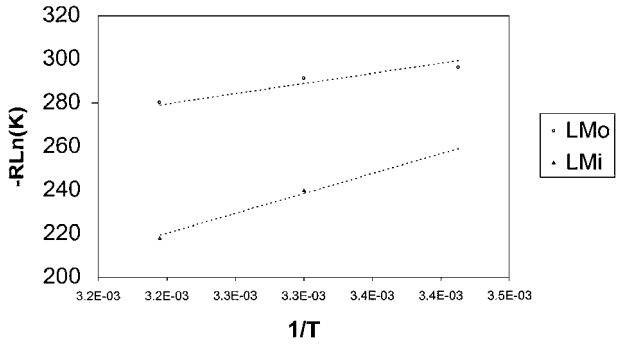

Figure 12 $-R$ Ln K versus $1/T$ for LM (inner and outer region) solid fly ash, based on $\overline{x_S}/x_{Si} = 0.990$ and $\overline{x_S}/x_{So} = 1.128$.

TABLE XII Thermodynamic properties, taken from Babushkin *et al.* [23] (with except of $HTiO_3^-$, which is taken from Paul [14]), and computed

	ΔH^0 (J/mole)	S^0 (J/mole K)	ΔG^0 (J/mole)
Literature			
H^+	0	0	0
OH^-	−229,999	−10.753	−157,277
AlO_2^-	−918,806	−20.92	−823,411
SiO_3^{2-}	–	–	−939,726
Ca^{2+}	542,665	−55.23	−552,706
Mg^{2+}	−461.746	−119.66	−455,261
Na^+	−240,454	−58.99	−262,211
K^+	−252,295	−102.17	−282,671
Fe^{3+}	−50,752	−279.07	−17,866
$HTiO_3^-$	–	–	−467,353
H_2O	−285,830	69.915	−237,178
SiO_2 (gl)	−901,568	46.861	−848,641
SiO_2 (β-quartz)	−911,066	41.840	−856,674
$2SiO_2 \cdot Al_2O_3$ (cr)	−3,378,412	124.18	−3,173,397
Computed			
EFA outer region (gl)			−1,547,777
LM outer region (gl)			−1,419,672
LM inner region (gl)			−1,419,112
LM outer region, redistributed (gl)			−1,400,889
LM inner region, redistributed (gl)			−1,412,041

in a position to determine the free energy, enthalpy and entropy of formation of LM and EFA glass phase. In Table XII, the free energy, enthalpy and entropy of formation (ΔG^0, ΔH^0 and S^0, respectively) of some substances are listed ($T = 298$ K), taken from Babushkin *et al.* [23] and Paul [14], employing 1 cal = 4.184 J. Unfortunately, from SiO_3^{2-} and $HTiO_3^-$ only ΔG^0 is available, so that it is only possible to determine ΔG^0 of the fly ash.

Firstly, ΔG of the EFA and LM reaction is computed at 298 K using Equation 51 and the fitted values of ΔH and ΔS as listed in Tables VI and VII. The resulting ΔG_{298} is being included in these tables as well. Considering reaction (40), ΔG^0 of EFA and LM glass now follow from:

$$\begin{aligned}\Delta G^0 = &-\Delta G_{298} - (2 + 2\alpha - 2\beta - 2\gamma - 6\delta + \varepsilon)\\ &\Delta G^0_{OH^-} + \Delta G^0_{SiO_3^{2-}} + 2\alpha\Delta G^0_{AlO_2^-}\\ &+ \beta\left(\frac{\bar{x}_C}{\bar{x}_C + \bar{x}_M}\Delta G^0_{Ca^{2+}} + \frac{\bar{x}_M}{\bar{x}_C + \bar{x}_M}\Delta G^0_{Mg^{2+}}\right)\\ &+ 2\gamma\left(\frac{\bar{x}_N}{\bar{x}_N + \bar{x}_K}\Delta G^0_{Na^+} + \frac{\bar{x}_K}{\bar{x}_N + \bar{x}_K}\Delta G^0_{K^+}\right)\\ &+ 2\delta\Delta G^0_{Fe^{3+}} + \varepsilon\Delta G^0_{HTiO_3^-}\\ &+ (1 + \alpha - \beta - \gamma - 3\delta)\Delta G^0_{H_2O}\end{aligned} \tag{53}$$

Taking $\bar{x}_C, \bar{x}_M, \bar{x}_N, \bar{x}_K, \alpha, \beta, \gamma, \delta$ and ε from Table VIII, the value of ΔG_{298} listed in Tables VI and VII, and taking the free energies of formation from Table XII, ΔG^0 is computed using Equation 53 and included in this table as well.

Note that in reaction (40), β and γ and represent the total molar content of earth alkalis and alkalis to molar content of silica, respectively. But to compute ΔG^0, the actual contents of MgO, CaO, Na_2O and K_2O have

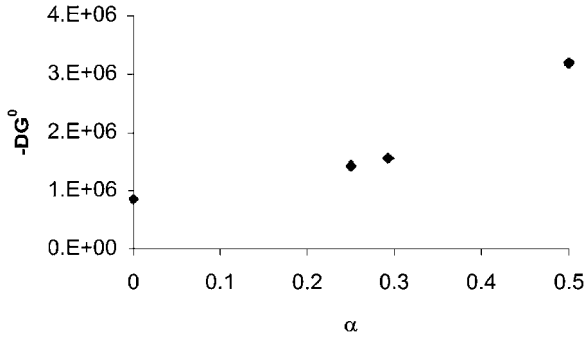

Figure 13 $-\Delta G^0$ versus α (A/S molar ratio).

to be accounted of. For that reason, the molar ratios $\bar{x}_C/(\bar{x}_M + \bar{x}_C)$ etc. are appearing in Equation 53.

For the computation of the redistributed (inhomogeneous) LM fly ash, now the values of α, β, γ, δ and ε from Table IX are used, and ΔG_{298} from Table XI. The ratios $\bar{x}_C/(\bar{x}_M + \bar{x}_C)$ etc., however, are taken to be the same as for the foregoing homogeneous LM fly ash computations (based again on Table VIII), i.e. it is assumed that MgO and CaO retain the same molar ratio, and the alkalis Na_2O en K_2O retain the same molar ratio. In other words, the outer region is enriched with alkalis and earth alkalis, but for MgO and CaO, and for Na_2O en K_2O, to the same extent. The resulting computed ΔG^0 are included in Table XII as well.

From this table one can conclude that with increasing α (i.e. *A/S* molar ratio) $-\Delta G^0$ increases. For EFA, α takes a value of about 0.29 and for LM about 0.25, and indeed, $-\Delta G^0$ of EFA is larger. Furthermore, one can see that for LM the values pertaining to inner and outer are very close. Also the redistribution as executed in the previous section (enriching of LM outer layer with K_2O, Na_2O, CaO, MgO, Fe_2O_3 and TiO_2, whereby α is not altered), yields values that are close to the values of homogeneous LM fly ash (all LM values differ less than 1.5%). From this information it can be concluded that $-\Delta G^0$ is mainly governed by α.

In order relate the computed values of $-\Delta G^0$ with values reported in literature, values of $-\Delta G^0$ of silica (quartz and vitreous, $\alpha = 0$) and of $2SiO_2 \cdot Al_2O_3$ ($\alpha = 0.5$) are also included in Table XII. One can see that $-\Delta G^0$ of LM and EFA are located between the values of silica and of $2SiO_2 \cdot Al_2O_3$. Moreover, they are in line with the trend that for larger α, $-\Delta G^0$ also increases, confirming the reliability of the computed values of $-\Delta G^0$. In Fig. 13, $-\Delta G^0$ is set out graphically against α, whereby the value of $-\Delta G^0$ is taken from vitreous silica and from EFA and LM outer regions (without redistribution).

For most fly ashes, α lies in the range 0.25–0.29. For these fly ashes a tentative value of $-\Delta G^0$ can be obtained from the values of LM and EFA determined here, e.g. by interpolation. For values in the range 0–0.25 and 0.29 to 0.5, interpolation between silica and LM and between EFA and $2SiO_2 \cdot Al_2O_3$, respectively, is recommended. The latter range generally holds for slags. A direct measurement of $-\Delta G^0$ would be more accurate, but also more elaborate. Interpolation as proposed here will readily provide a value that can be useful for tentative reactivity computations.

8. Conclusions

Pietersen [7, 8] has carefully executed and reported dissolution experiments of several types of pulverised powder coal (class F) fly ashes. To this end, the silica release in time was measured for various pOH and temperatures. In order to understand the dissolution and reaction behaviour of these fly ashes, in particular the EFA and LM fly ash, a theoretical study has been executed and the results applied to said experiments.

From the present analysis one can confirm that the available amount of reactive fly ash is proportional to the glass (non-crystalline) part of the fly ash. Moreover, as the crystalline part forms a connected network, dissolution rates are also proportional to the glass content, especially while the effective diffusion coefficient is proportional to the square of the glass content (Equation 2).

The derivation of an extended shrinking core model yields analytical equations that reckon with a hollow core, as well as the possibility of two regions with different composition and reactivity. In Fig. 8 the shrinking behaviour in case of a more and less reactive outer region has been depicted. Application of the derived equations to the experiments of Pietersen [7, 8] provides values of the reactivity time τ (Equation 10) for inner and outer region (τ_i and τ_o). Assuming a homogeneous silica distribution over the fly ash particle, the application reveals that the inner region is more reactive, and that about 7% and 9% of the silica is found in the outer region of LM and EFA solid spheres, respectively. From the fitting it also follows that the outer region of solid spheres and cenospheres have nearly the same thickness (about 2 μm). After dissolution of this layer, which needs less time in case of higher pH and/or temperature, the dissolution of the inner region at a higher rate starts.

Furthermore, a reaction mechanism for fly ash glass is put forward that accounts for its mineral composition (silica, aluminium oxide, iron oxide, titanium oxide, alkali and earth alkali content) and which also could be useful for slags. The resulting reaction product and the experimental application indicate a dissolution rate proportional to $[OH^-]^{0.9-1}$ for the outer region (EFA and LM), and to $[OH^-]^{1.4}$ in inner region (information available about LM only). This result suggests that the outer layer of solid LM is poorer in silica and aluminiumoxide, which is in line with findings in previous publications. As most information is obtained for solid LM, for this fly ash the silica and aluminiumoxide is concentrated in the inner region, and the model again applied, providing values that more closely correspond to the trends found.

Combining the reaction product and the experimental data at various temperatures, also the free energy, enthalpy and entropy of reaction are computed of EFA and LM glass phase. Finally, these data are used to compute the free energy of formation ΔG^0 of both glasses. It follows that the free energy of formation is mainly governed by the molar ratio (α) of the major constituents SiO_2 and Al_2O_3. The values obtained are in line with those of known substances, silica ($\alpha = 0$) and $2SiO_2 \cdot Al_2O_3$ ($\alpha = 0.5$). With this information one

can assess ΔG^0 of (fly ash and slag) glass phases with deviating A/S molar ratio, and subsequently, to assess their reactivity in a cement environment.

References

1. A. L. A. FRAAY, J. M. BIJEN and Y. M. DE HAAN, *Cement and Concrete Res.* **19** (1989) 235.
2. A. XU and S. L. SARKAR, *J. Mat. in Civil Eng.* **6** (1994) 117.
3. H. F. W. TAYLOR, "Cement Chemistry," 2nd edn. (Thomas Telford, London, 1997).
4. P. C. HEWLETT, "Lea's Chemistry of Cement and Concrete," 4th edn. (Arnold, London, 1998).
5. S. SONG and H. M. JENNINGS, *Cement and Concrete Res.* **29** (1999) 159.
6. S. SONG, D. SOHN, H. M. JENNINGS and T. O. MASON, *J. Mater. Sci.* **35** (2000) 249.
7. H. S. PIETERSEN, in *Mat. Res. Soc. Symp. Proc.*, Vol. 178, Materials Research Society, 1990, p. 139.
8. *Idem.*, Ph.D. Thesis, Delft University of Technology, The Netherlands, 1993.
9. S. YAGI and D. KUNII, in Proc. 5th Int. Symp. on Combustion, 1955.
10. H. S. PIETERSEN, private communications, 2000.
11. L. D. HULETT and A. J. WEINBERGER, *Env. Sci and Technology* **14** (1980) 965.
12. R. T. HEMMINGS and E. E. BERRY, in *Mat. Res. Soc. Symp. Proc.*, Vol. 113, Materials Research Society, 1988 p. 3.
13. O. LEVENSPIEL, "Chemical Reaction Engineering," 3rd edn. (John Wiley, New York, 1999).
14. A. PAUL, *J. Mater. Sci.* **12** (1977) 2246.
15. *Idem.*, "Chemistry of Glass," 2nd edn. (Chapman, London, 1990).
16. F. G. HELFFERICH, "Ion Exchange" (Dover, New York, 1995).
17. F. A. L. DULLIEN, "Porous media: Fluid transport and Pore Structure" (Academic Press, New York, 1979).
18. N. WAKAO and J. M. SMITH, *Chem. Eng. Sci.* **17** (1962) 825.
19. M. POURBAIX, "Atlas of Electrochemical Equilibria in Aqueous Solutions" (Pergamon, Oxford, 1966).
20. D. E. MACPHEE and F. P. GLASSER, *MRS Bulletin* **18**(3) (1993) 66.
21. R. D. SMITH, *Prog. Energy Combust. Sci.* **6** (1980) 53.
22. D. R. L. LIDE (ed.), "CRC Handbook of Chemistry and Physics," 76th edn. (CRC Press, Boca Raton, 1995).
23. V. I. BABUSHKIN, G. M. MATVEYEV and O. P. MCHEDLOV-PETROSSYAN, "Thermodynamics of Silicates" (Springer, Berlin, 1985).

Received 28 June 2000
and accepted 28 August 2001